The Low-Lying Electronic States of Pentacene and Their Roles in Singlet Fission

ARTICLE *in* JOURNAL OF THE AMERICAN CHEMICAL SOCIETY · APRIL 2014

Impact Factor: 12.11 · DOI: 10.1021/ja500887a · Source: PubMed

3 AUTHORS, INCLUDING:

Tao Zeng
Carleton University
41 PUBLICATIONS **295** CITATIONS

SEE PROFILE

JACS
JOURNAL OF THE AMERICAN CHEMICAL SOCIETY
Article
pubs.acs.org/JACS

The Low-Lying Electronic States of Pentacene and Their Roles in Singlet Fission

Tao Zeng, Roald Hoffmann, and Nandini Ananth*

Department of Chemistry and Chemical Biology, Cornell University, Ithaca, New York, 14853, United States

Supporting Information

ABSTRACT: We present a detailed study of pentacene monomer and dimer that serves to reconcile extant views of its singlet fission. We obtain the correct ordering of singlet excited-state energy levels in a pentacene molecule ($E(S_1) < E(D)$) from multireference calculations with an appropriate active orbital space and dynamical correlation being incorporated. In order to understand the mechanism of singlet fission in pentacene, we use a well-developed diabatization scheme to characterize the six low-lying singlet states of a pentacene dimer that approximates the unit cell structure of crystalline pentacene. The local, single-excitonic diabats are not directly coupled with the important multiexcitonic state but rather mix through their mutual couplings with one of the charge-transfer configurations. We analyze the mixing of diabats as a function of monomer separation and pentacene rotation. By defining an oscillator strength measure of the coherent population of the multiexcitonic diabat, essential to singlet fission, we find this population can, in principle, be increased by small compression along a specific crystal direction.

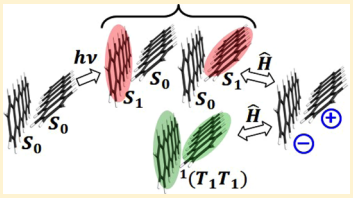

INTRODUCTION

Singlet fission (SF) is the process by which one singlet exciton, generated in a material by absorbing one photon, splits into two triplet excitons.[1,2] The low-lying singlet-coupled state of the two triplet excitons may be accessible and close in energy to the initially excited singlet, making SF a spin-allowed process. The ensuing doubling of photon-to-electron conversion efficiency appears to be a promising pathway to surpass the Shockley–Queisser conversion limit (about 30%)[3] for single junction solar cells.[4−6]

SF has been extensively studied in polyacenes, a family of hydrocarbons that are formed by linearly fusing benzene rings. In 1965, SF was first proposed to explain the relatively weak and delayed fluorescence in anthracene (three rings) single crystals.[7] It was invoked again in the next few years to explain fluorescence quenching and triplet exciton generation in crystalline tetracene (four rings).[8,9] These early examples clearly demonstrated the potential benefit of SF in photovoltaic materials: SF competes with, and indeed quenches the fluorescence of the photogenerated singlet exciton, and yields two triplet excitons. Fluorescence of these triplet excitons to the singlet ground state is spin forbidden, making them longer-lived and allowing them greater diffusion length scales that in turn help them reach the interface between the light-harvesting material and an electron acceptor (e.g., C_{60}). At the interface, each exciton potentially transfers an electron to the acceptor, resulting in the generation of two free charge carriers.

From a thermodynamic point of view, to facilitate SF:

$$S_0 \xrightarrow{h\nu} S_1 \rightarrow \cdots \rightarrow 2T_1 \quad (1)$$

a material should satisfy the exoergicity criterion $E(S_1) - 2E(T_1) \geq 0$,[10] or at least not fall far from it. Here, S and T are used to label singlet and triplet excited or excitonic states, the subscript 1 is used to denote the first excited state in the respective spin manifolds, the subscript 0 indicates the ground state, and "⋯" indicates the intermediate steps in SF that are the subject of our study. As the number of rings in polyacenes increases, they satisfy the energy criterion better;[11] the endoergicities of SF for anthracene,[12,13] tetracene,[14] and pentacene[15−17] crystals have been determined to be 0.53, 0.18, and −0.11 eV respectively; pentacene (**1**) is thus the smallest acene where SF is exoergic. Experimental studies using transient absorption spectroscopy reveal that SF in pentacene occurs on a time scale of ∼100 fs.[18−21]

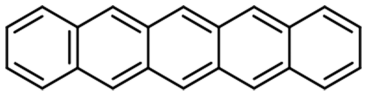

1

In identifying the mechanism of SF, a first step is the investigation of the low-lying excited states of a pentacene molecule. Despite significant advances in electronic structure methods, the large size of pentacene limits the accuracy and reliability of methods that can be used to obtain the detailed electronic-state information necessary to characterize SF.[1] Previous studies include work by Paci et al. where time-dependent density functional theory (TD-DFT) is used to calculate the relative energetics of the S_1, T_1, and T_2 states of a pentacene molecule.[5] Pabst and Köhn used an approximate coupled-cluster singles and doubles model (CC2) to calculate the $T_1 \rightarrow T_n$ excitation energies of pentacene.[22] However, more accurate results require multireference electronic structure methods.[23,24] In the first such study,[25] Zimmerman et al. used

Received: January 26, 2014
Published: March 16, 2014

   dx.doi.org/10.1021/ja500887a | J. Am. Chem. Soc. 2014, 136, 5755−5764

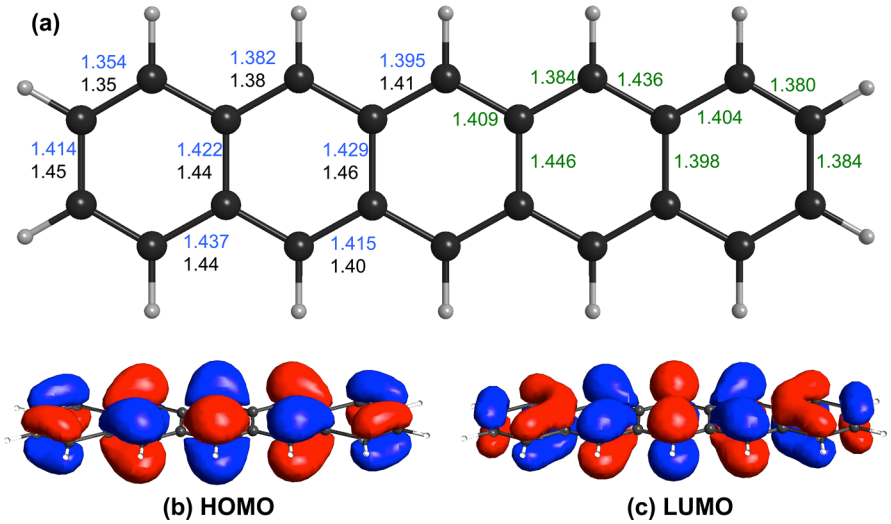

Figure 1. (a) Symmetrically unique C−C bond lengths of our CASSCF/12π12e optimized structure for the ground (blue) and the lowest triplet (green) states in comparison with experimental values (black) taken from ref 52. (b) HOMO and (c) LUMO of pentacene.

multireference Møller−Plesset perturbation theory (MRMP)[26−28] to investigate the low-lying states of pentacene. Their work identifies the lowest-lying excited state as a doubly excited state corresponding to two triplet excitons effectively generated within one molecule. This finding, however, contradicts experimental observations.[1,2,29,30]

The mechanism of SF in acenes, i.e., the detailed steps in eq 1, requires a model that includes two or more molecules. An early kinetic model proposed by Merrifield and Johnson and elaborated by Suna,[31−33] aimed to explain the mutual annihilation of triplet excitons, describes SF as a stepwise process:

$$S_0 \xrightarrow{h\nu} S_1 \underset{k_{-2}}{\overset{k_2}{\rightleftharpoons}} {}^1(T_1T_1) \underset{k_{-1}}{\overset{k_1}{\rightleftharpoons}} T_1 + T_1 \tag{2}$$

where ${}^1(T_1T_1)$ corresponds to a singlet state formed by the intimate spin-coupling of two T_1 excitons. The rate coefficients in eq 2 k_2 (k_{-2}) describe the formation (annihilation) of the coupled triplet excitons and k_1 (k_{-1}) measure the rates of the disentanglement and separation (entanglement and approach) of the two triplets. However, recent time-resolved two-photon photoemission (TR-2PPE) spectroscopic experiments on crystalline tetracene[34] and pentacene[35] suggest the simultaneous formation of the ${}^1(T_1T_1)$ and S_1 states via a coherent mechanism:[36]

$$S_0 \xrightarrow{h\nu} [S_1 \Leftrightarrow {}^1(T_1T_1)] \tag{3}$$

In an effort to qualitatively explain these findings, recent theory has focused on three kinds of diabatic states involved in SF for dimers: local single-excitations on one molecule, charge-transfer states, and singlet-coupled multiexciton states with two triplets located on different molecules.[37−42] An expression for the Hamiltonian matrix elements between these states has been formulated by Smith and Michl using a minimum configuration space.[1] Calculations for specific systems include that of Difley and Van Voorhis who employed different DFT schemes (TD- and constrained DFT) to approximate the diabats and calculate their coupling matrix element, for the dimer of triphenylene and 1,3,5-trinitrobenzene;[43] Havenith et al. employed a nonorthogonal configuration interaction method to calculate the diabatic states and their Hamiltonian couplings for a tetracene trimer;[44] Berkelbach et al. approximated the couplings between the diabats using Fock matrix elements of the HOMO and LUMO on two pentacene molecules;[41] Beljonne et al. employed a similar scheme to investigate the Davydov splitting and SF in pentacene.[42] Feng et al. investigated the possible nonadiabatic coupling between the single- and multiexciton states for tetracene and pentacene dimers.[45] More recently, the same group proposed a simple kinetic model for SF that elucidates the role of entropy in SF.[46] Kuhlman et al. used a combination of TD-DFT and quantum mechanics/molecular mechanics (QM/MM) to investigate the excited states of a pentacene dimer in a crystalline environment and proposed an internal conversion mechanism for SF in this system.[11] Zimmerman et al. performed complete active space self-consistent field (CASSCF) calculation on a symmetric pentacene dimer to identify a low-lying multiexciton state and suggested a nonadiabatic mechanism for the transition from the S_1 state to the ${}^1(T_1T_1)$ state.[25] In a follow-up study, the proposed nonadiabatic mechanism was further examined for a dimer structure from crystalline pentacene, with restricted active-space spin-flip method (RAS-SF) calculation.[47,48]

The first objective of this paper is to investigate the low-lying excited states of the pentacene molecule. The second objective is to reconcile the quite differing extant views of the mechanism of SF in a pentacene dimer using multireference methods based on wave function theory that include both nondynamical and dynamical correlations. Our third objective is to accurately calculate diabatic states and provide a clear physical picture of the roles of the three different kinds diabats thought to participate in pentacene SF. In this work, we confine our picture of SF to the steps from photoabsorption to the occupation of the singlet-coupled triplet−triplet state, ${}^1(T_1T_1)$. The further decoherence of the coupled triplets is left for a future quantum dynamics study.

■ ENERGY ORDERING OF EXCITED STATES OF A PENTACENE MOLECULE

In choosing the active space for our multireference calculations we are guided by the work of Kawashima et al.[24] who calculated the valence $\pi\rightarrow\pi^*$ excitation spectra for anthracene and tetracene using a 12π12e (12 π orbitals, 12 electrons) active

dx.doi.org/10.1021/ja500887a | J. Am. Chem. Soc. 2014, 136, 5755−5764

space and the MRMP method to obtain good agreement with experimental measurements. All computations in this section are done in a state-specific manner unless further specified. We optimize the monomer structures for the lowest singlet and the lowest triplet states at the level of CASSCF/12π12e. As Figure 1a shows, the C−C bond lengths of the ground state are in reasonable agreement with experiment, with the largest deviations occurring for the "cross-ring" bonds. We then calculate the excitation energies using the MRMP/12π12e scheme. Singlet energies are calculated using the S_0 optimized structure and triplet energies obtained using the T_1 structure. This selection of structures is consistent with the experimental excitation energies cited below: $E(S_1)$ is a vertical $S_1 \leftarrow S_0$ excitation energy;[49] $E(T_1)$ is obtained through a kinetic model for heterofission of pentacene dopant in tetracene host,[17] corresponding to an adiabatic excitation energy; $E(T_2)$ is estimated from photoinduced $T_2 \leftarrow T_1$ excitation,[50,51] corresponding to a sum of the adiabatic $T_1 \leftarrow S_0$ and vertical $T_2 \leftarrow T_1$ excitation energies.

Our calculated excitation energies, shown in the second column of Table 1, are in excellent agreement with experimental values provided in column 1. We further examine our MRMP states to see whether they have balanced reference weights. The reference weight measures the percentage of the reference CASSCF state in the final state that is perturbed to the second order; it is an indicator of the quality of the zeroth-order wave function.[53] The reference weights from our calculation shown in parentheses in column 2 of Table 1 are all 44−46% indicating the balanced contributions from perturbation in our wave functions and energies;[54] the relatively low magnitude of the reference weights is expected given the large size of the molecule and the approximate size consistency of the MRMP method. In addition, we find all the active orbitals are substantially occupied (e.g., the minimum occupation numbers are 0.0428 and 0.0553 in the S_0 and D states) confirming an appropriate choice of the 12π12e active space. We further calibrate the accuracy of our MRMP results by checking for an intruder state problem.[55,56] We find that all the weights and excitation energies remain largely the same after the intruder state avoidance (ISA) shifting[55,56] is introduced, with the conventional shifting parameter of 0.02 E_H^2. These invariances suggest no intruder state problem in our calculations.

Table 1. Calculated Excitation Energies (in eV) and Reference Weights (in parentheses) of the Low-Lying States of the Pentacene Molecule

		1	2	3	4
state	symmetry	Exp.[a]	12π12e[b]	12o12e[c]	2o2e[d]
S_0	^1A_g	0.0	0.00 (46%)	0.00 (45%)	0.00 (50%)
S_1	$^1B_{2u}$	2.3	2.31 (45%)	2.05 (44%)	2.24 (48%)
D	^1A_g	?	2.63 (44%)	1.95 (36%)	–
T_1	$^3B_{2u}$	0.86	0.87 (46%)	0.87 (45%)	1.14 (48%)
T_2	$^3B_{1g}$	>2.0	2.07 (45%)	2.25 (41%)	–

[a] S_1 experimental excitation energy is taken from ref 49, T_1 from ref 17, and T_2 from refs 50 and 51. [b] All singlet (triplet) energies are calculated at the CASSCF/12π12e optimized structure for the lowest singlet (triplet) state. [c] Vertical excitation energies from our reproduction of the calculations of ref 25. [d] MRMP/2o2e Vertical excitation energies using the ground-state structure from CASSCF/12π12e optimization. ISA shifting is employed. Reference states are prepared in a state-averaged manner, averaging S_0, S_1, and T_1 states.

The lowest singlet excited state of the pentacene molecules is the $^1B_{2u}$ state mainly (84%) formed by a HOMO-to-LUMO (Figure 1b,c) single excitation. There is a second singlet excited state, ^1A_g, about 0.3 eV higher in energy, that arises from double excitations: 48% HOMO to LUMO, 7% HOMO−1 to LUMO, and 6% HOMO to LUMO+1. Since excitation to this state is symmetry forbidden, it is a dark state and has been labeled D in the literature;[25] this state is a common feature of polyene spectroscopy.[57,58] The energy ordering of these two singlet excited states from our calculations is $E(S_1) < E(D)$, in line with the ordering found experimentally.[1,2,29,30]

We performed additional calculations to understand the different energy ordering reported by Zimmerman et al. who found $E(D) < E(S_1)$.[25] Their energy ordering suggests that the D state should be involved in the dynamics of pentacene SF.[59] We reproduce their excitation energies as closely as possible, and we also calculate the reference weight for each state as shown in the third column of Table 1. A detailed analysis shows that the central difference is in the choice of active space: Zimmerman et al. employ a 12o12e ("o" for general orbitals) active space with 10 π-type and 2 non-π-type (these appear to be of a Rydberg type) orbitals, whereas our 12 orbital active space contains only π-type orbitals. We note the low (36%) weight of the D state in our reproduction of Zimmerman et al.'s calculations. We believe that the inclusion of the almost empty Rydberg orbitals (with occupation numbers <0.002) in the active space introduces an intruder state problem. When we apply an ISA shifting[55,56] to correct this problem, we obtain balanced reference weights along with an energy ordering identical to the 12π12e results in column 2 of Table 1, i.e., $E(D) > E(S_1)$. These calculations confirm that the D state need not be considered in the discussion of SF in pentancene. Further details of these monomer calculation results are given in Section S.1 of the Supporting Information (SI).

The S_1 and T_1 states of pentacene mainly involve HOMO-to-LUMO single excitation; 77% of our T_1 state is described by such an excitation. We use this character to explore the possibility of reducing the orbital active space to include only the HOMO and LUMO of the molecule, an assumption that is implicitly made in several recent theoretical studies.[38,40−42,45,47] Such reduction is necessary to enable multireference calculations on a pentacene dimer. We calculate the vertical excitation energies of the S_1 and T_1 states using an MRMP/2o2e scheme where the 2o refers to the HOMO and LUMO orbitals. The S_1 excitation energy (column 4 of Table 1) is in satisfactory agreement with the experimental result, while the T_1 energy (1.14 eV) is 0.28 eV different. This discrepancy comes from the fact that we are comparing vertical (2o2e calculation) and adiabatic, experimental excitations[17] for the T_1 state. The MRMP/12π12e vertical excitation energy of the T_1 state is 1.07 eV (column 6 of Table S.1 in the SI), and the 2o2e value is only greater than it by 0.07 eV. We note that the vertical excitation energy is of more relevance in subsequent calculations of dimer models, where a frozen structure approximation is employed. Also, the satisfactory MRMP/2o2e excitation energies support the adequacy of the more cost-effective basis set, SBKJC+d (see Computational Methods section for further details), which is used in the calculations below.

Within this economical calculation, $2 \times E(T_1)$ is slightly greater than $E(S_1)$, although the close-to-resonance relation

dx.doi.org/10.1021/ja500887a | J. Am. Chem. Soc. 2014, 136, 5755−5764

between $E(S_1)$ and $2E(T_1)$ is retained. However, if eq 1 proceeds through a coherent mechanism (*vide infra*), the thermodynamic condition of $E(S_1) \geq 2E(T_1)$ may not be as important as it was thought in the population of $^1(T_1T_1)$ dimer state.

ROLES OF LOW-LYING STATES IN PENTACENE SINGLET FISSION

The study of SF in pentacene requires a model with more than one molecule; the minimal model for the process is a dimer, which we now proceed to analyze. To build a dimer model, we combine our CASSCF/12π12e optimized S_0 monomer geometry with the TOPAS (the trade name for Ticona cyclo-olefin copolymers) substrate thin film intermolecular configuration.[52] This configuration is also used in the theoretical study of Kuhlman et al.[11] We call this structure, shown in Figure 2, the reference dimer structure, with the two monomers

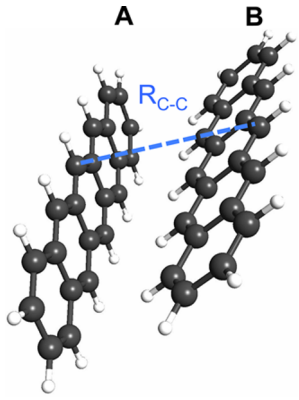

Figure 2. Arrangement of two monomers in a unit cell of the pentacene crystal thin film structure on a TOPAS substrate.[52] Black and white spheres represent carbon and hydrogen atoms. Also shown is the R_{C-C} distance of the dimer.

labeled A and B. Similar models to study pentacene SF, without the surrounding molecules in real crystals, have been used in refs 41, 42, and 45. We note that pentacene SF is observed to occur within a very short time (~80 fs) after initial photoexcitation,[35,36] allowing us to assume that the monomer structure is frozen during SF.

Although our dimer model captures the most essential structural features of the pentacene crystal unit cell, it does not account for solid-state effects that can lead to greater separation between monomers and a different dielectric constant. We believe, however, that this will not affect our central conclusions regarding the mechanism of SF in pentacene.

In the previous section we established the sufficiency of a 2o2e active space for each monomer. Accordingly, state-averaged extended multiconfigurational quasi-degenerate perturbation theory (XMCQDPT) calculations with an active space of 4o4e (HOMOs and LUMOs on the two monomers) are performed to obtain the adiabatic energies and wave functions for the six lowest singlet states for a given dimer structure. ISA shifting is employed. The six singlet adiabatic states are labeled S_0^d, ..., and S_5^d, where the superscript d denotes that they are dimer states (distinct from the monomer states discussed above), and the subscript denotes the ordinal energy ordering.

We use only six singlets for the dimer, assuming that (and here we follow Smith and Michl)[1] it takes six prototype diabatic configurations to describe the essence of SF when both S_1 and T_1 involve only HOMO-to-LUMO excitation. These prototype configurations are schematically shown in Figure 3a and include

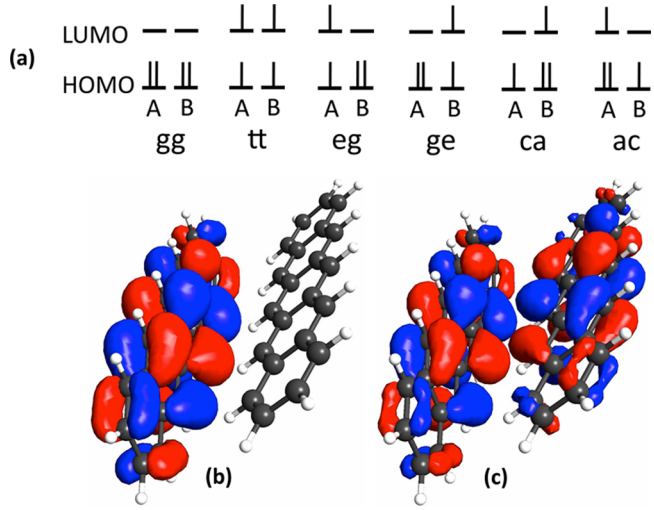

Figure 3. (a) Schematic illustration of the six diabats (prototypes) involved in the pentacene SF. Vertical bars stand for electrons, while horizontal bars for molecular orbitals. "A" and "B" denote the two monomers in Figure 2. (b) A diabatic molecular orbital (DMO) of the dimer that has clear character of the HOMO on one monomer (compare with Figure 1b). (c) A canonical molecular orbital of the dimer, mainly composed of HOMOs on the two monomers.

the ground state, *gg*, local single-excitons, *eg* and *ge*, charge-transfer configurations, *ca* and *ac*, and the singlet-coupled triplet−triplet state, *tt*. In the diabatic state labels, the first letter corresponds to monomer unit A and the second to monomer unit B, and we use the notation *g* for ground state (like S_0), *t* for triplet (like T_1), *e* for a local excitation of one monomer (like S_1), *c* for cation, and *a* for anion formation of a monomer.

The "real" diabatic states in our calculation are obtained from the adiabatic singlet states of the dimer by applying a unitary transformation that maximizes the character of one prototype configuration in one diabat.[60] Specifically, we employ the four-fold scheme of Nakamura and Truhlar.[61,62] Such a direct diabatization includes both one- and two-electron contributions in the diabatic couplings. Our diabatic molecular orbitals (DMOs), one of which is shown in Figure 3b, are obtained by rotating all active orbitals, one of which is shown in Figure 3c, to satisfy the maximum overlap reference molecular orbitals criterion.[61,62] The reference MOs are obtained from restricted open-shell Hartree-Fock (ROHF) calculations on the dimer at a large (20 Å) intermolecular distance; each DMO can be unambiguously associated with a frontier orbital of one monomer; the monomer DMOs are used to generate the diabatic configurations in Figure 3a.

Feng et al. have argued that it is not possible to represent the low-lying adiabatic states of the dimer by a few diabats, as used here, since their contributions do not add up to 100%.[45] All practical diabatization schemes, however, only yield quasi-diabatic states that change smoothly with nuclear configuration and maintain their chemical characters as much as possible.[60,63,64] In almost all calculations shown here, the contributions of the six prototype configurations in Figure 3a add up to more than 92% of the six adiabatic states, leading us

dx.doi.org/10.1021/ja500887a | J. Am. Chem. Soc. 2014, 136, 5755−5764

to believe that our diabatization scheme can provide a quantitative understanding of SF.

Analyzing Interactions between the Diabatic States at the Reference Dimer Structure. We investigate the interactions between diabatic states of the pentacene dimer at its reference geometry to understand their roles in SF. The Hamiltonian matrix in the basis of the six diabatic states labeled by their dominant prototype configurations is

$$\begin{array}{c} \\ gg \\ tt \\ eg \\ ge \\ ac \\ ca \end{array} \begin{array}{c} \begin{array}{cccccc} gg & tt & eg & ge & ac & ca \end{array} \\ \begin{pmatrix} 0 & 4 & -1 & -20 & 69 & -91 \\ 4 & 1900 & 0 & 1 & -90 & 64 \\ -1 & 0 & 2005 & -6 & 99 & 79 \\ -20 & 1 & -6 & 2010 & 75 & 86 \\ 69 & -90 & 99 & 75 & 2266 & 1 \\ -91 & 64 & 79 & 86 & 1 & 3063 \end{pmatrix} \end{array} , \quad (4)$$

where all energies are in units of meV, and the diagonal elements are shifted such that $E(gg)$ is 0 meV. Qualitatively similar matrices were constructed in refs 41 and 42, including only one-electron coupling. From our XMCQDPT calculation, the magnitudes of the *tt-ca*, *tt-ac*, *eg-ca*, *eg-ac*, *ge-ca*, and *ge-ac* couplings are all below 100 meV and are, as expected, smaller than the 100−160 meV values obtained from the Hartree−Fock approximation used in ref 41. The couplings that stem from two-electron interactions, such as *tt-eg*, *tt-ge*, *eg-ge*, and *ac-ca*, are <6 meV, validating previous assumptions that they are negligible in comparison with the couplings that arise mainly from one-electron interactions.[1,2] The *ac* (*ca*) diabat lies about 300 (1000) meV above the *tt*, *eg*, and *ge*. The large energy difference between *ca* and *ac* arises from the asymmetric geometrical alignment of the two monomers and was also noted by Beljonne et al.[42] We provide a detailed explanation of this energy difference in Section S.2 in the SI.

The adiabatic states are linear combinations of the six diabats,

$$\begin{aligned} |S_0^d\rangle &= 1.00|gg\rangle - 0.00|tt\rangle + 0.00|eg\rangle + 0.01|ge\rangle - 0.03|ac\rangle + 0.03|ca\rangle; \\ |S_1^d\rangle &= 0.02|gg\rangle + 0.92|tt\rangle - 0.20|eg\rangle - 0.15|ge\rangle + 0.29|ac\rangle - 0.02|ca\rangle; \\ |S_2^d\rangle &= 0.01|gg\rangle - 0.32|tt\rangle - 0.71|eg\rangle - 0.56|ge\rangle + 0.26|ac\rangle + 0.11|ca\rangle; \\ |S_3^d\rangle &= 0.01|gg\rangle - 0.01|tt\rangle + 0.62|eg\rangle - 0.78|ge\rangle - 0.01|ac\rangle + 0.02|ca\rangle; \\ |S_4^d\rangle &= -0.03|gg\rangle + 0.20|tt\rangle - 0.27|eg\rangle - 0.20|ge\rangle - 0.92|ac\rangle + 0.03|ca\rangle; \\ |S_5^d\rangle &= 0.03|gg\rangle - 0.05|tt\rangle - 0.07|eg\rangle - 0.08|ge\rangle - 0.01|ac\rangle - 0.99|ca\rangle. \end{aligned} \quad (5)$$

The percentage weights of the diabatic states comprising each adiabatic state at the reference geometry are provided in Table 2, along with the adiabatic energies. Note that at the reference structure, there are four excited states (S_1^d−S_4^d), quite different in character, within 0.5 eV of each other. If more pentacene units were included in the model, a band of states would evolve. In consideration of SF, it is unlikely that one could focus on a single excited state.

The energy difference between S_2^d and S_3^d, the two states with substantial *eg* and *ge* components, is 0.062 eV. Following a referee's suggestion, we note that this energy, after being scaled by 4exp(−1), gives 0.091 eV and is not far from the 0.12 eV experimental Davydov splitting of pentacene crystal.[65,66] The factor of 4 comes from an increase in the splitting due to the four nearest neighbors for each pentacene in the crystal. The exp(−1) is a reduction factor comes from vibronic coupling, with the approximate Huang−Rhys factor 1.[67] We calculate the transition dipole moments for $S_2^d \leftarrow S_0^d$ and $S_3^d \leftarrow S_0^d$ to be (5.75, −0.16, −0.24) and (0.62, 3.46, 0.37) debyes, respectively, in the crystal *abc*-frame. This is consistent with the earlier finding that the transitions to the Davydov-split pair of excitation are mainly polarized in the crystal *ab*-plane, with the lower component along the *a*-axis and the higher along the *b*-axis.[67] We note the *a*- and *b*-axes are oppositely defined in the present paper (and ref 52) and ref 67; our *a*-axis contains the nearest equivalent neighbors and corresponds to the *b*-axis in ref 67.

As eq 1 indicates, the first step of the overall SF process is photoexcitation from S_0^d to one or more low-lying singlet states. To gauge the likelihood (intensity) of this transition, we consider the oscillator strength between S_0^d and the other five adiabatic states. The *gg* diabat forms the overwhelming component of the S_0^d state, as shown in Table 2. At the reference geometry, the energy of the *gg* diabat is separated from the others by more than 1.5 eV, as shown in eq 4, and this is true at all geometries. We can, therefore, associate the S_0^d-to-S_i^d oscillator strengths with transitions between *gg* and the other five diabatic states.

The transition dipole moment between *gg* and *tt* is zero since a double excitation is involved and the dipole operator is a one-electron operator. The transition dipole moments between the *gg* and the two charge-transfer diabats are expected to be small because they involve transitions between the HOMO and LUMO on different monomers as shown in Figure 3a. Clearly, the *gg*-to-*eg* and *gg*-to-*ge* diabatic transitions are the main contributors to the S_0^d-to-S_i^d oscillator strengths. Therefore, populating the multiexciton state via a coherent mechanism such as the one proposed by Chan et al.[35,36] requires either direct or indirect coupling between the single- and multiexciton diabats, i.e., an excited adiabatic state with substantial contributions from both the *tt* and *eg*/*ge* diabats.

The negligibly small *tt-eg* and *tt-ge* Hamiltonian couplings (∼ 1 meV) and the relatively large energetic separation (∼ 110 meV) between the *tt* and *eg*/*ge* diabats exclude the likelihood of a direct coupling between them. Indirect coupling through the charge-transfer diabats seems to be the only viable scheme.[1,2,44] The *ca* and *ac* states have similar magnitude couplings with the *tt*, *eg*, and *ge* states, but the energy of the *ac* state is lower than the *ca* state, indicating that the indirect *tt-eg*/*ge* couplings should be mainly mediated by the *ac* diabat. Further, based on the decomposition of adiabatic states presented in Table 2, we note that S_5^d is derived primarily from the *ca* diabat, and S_3^d is a nearly pure excitonic state, with very little *tt* and charge-transfer character. The states with substantial mixing between *tt*, *eg*, and *ge*, such as S_1^d, S_2^d, and S_4^d, all have a sizable *ac* component. We conclude that only one of

Table 2. Energies[a] (in eV) and Percentage Weights (%) of the Six Diabats in the Six Singlet Adiabatic States at the Reference Structure

	energy	*gg*	*tt*	*eg*	*ge*	*ac*	*ca*
S_0^d	0.000	99.8	0.0	0.0	0.0	0.1	0.1
S_1^d	1.875	0.0	85.6	4.0	2.2	8.2	0.0
S_2^d	1.956	0.0	10.3	50.0	31.6	6.9	1.3
S_3^d	2.018	0.0	0.0	38.4	61.6	0.0	0.0
S_4^d	2.337	0.0	3.8	7.2	4.0	85.0	0.0
S_5^d	3.087	0.0	0.3	0.5	0.7	0.0	98.5

[a]All energies are relative to the ground-state energy at the reference structure.

dx.doi.org/10.1021/ja500887a | J. Am. Chem. Soc. 2014, 136, 5755−5764

the charge-transfer states, the *ac* diabat, mediates the coupling between the multi- and single-exciton diabats.

We note that the indirect *tt-eg/ge* coupling is switched on by lowering the symmetry of the dimer. For example, were the dimer to have a parallel sandwich D_{2h} structure, the *tt* state and the Davydov split pair of single-exciton states, $(1/2)^{1/2}(|eg\rangle \pm |ge\rangle)$, would transform as A_g, B_{3g} and B_{1u}, respectively.[45] As long as the D_{2h} symmetry is maintained, there will be no *tt-eg/ge* coupling, direct or indirect. The dimer in the pentacene crystal unit cell has a C_1 symmetry. Consequently, all diabatic states transform as the same irreducible representation, *A*, and can undergo mixing.

Structural Effects on the Pentacene Singlet Fission: Intermolecular Distance. We define the intermonomer distance, R_{C-C}, as the distance between the middle carbon atoms at the far edges of the monomers shown in Figure 2, following previous work.[42,47] Our reference dimer geometry has R_{C-C} = 5.9 Å. The energies of the adiabatic and diabatic excited states are shown in Figure 4a and the important Hamiltonian

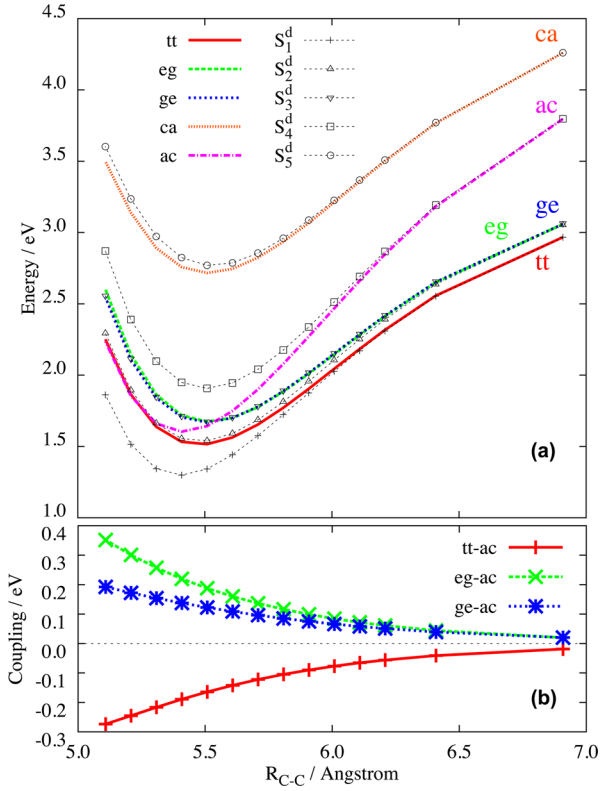

Figure 4. (a) Energies of the five diabatic states and five excited adiabatic states. (b) Important couplings between the diabats along R_{C-C}. All energies in (a) are differential energies with respect to the S_0^d energy at the reference geometry, R_{C-C} = 5.9 Å. Note that the energy scale in (b) is quite different from (a).

couplings between diabats in Figure 4b. We note that S_5^d and S_3^d have energy curves close to the *ca* and *eg/ge* diabats, respectively, over almost the entire range of monomer separations (Figure 4a). For S_5^d, this is due to its dominant *ca* character. The explanation for S_3^d closely following the *eg/ge* diabatic energy curves is a little more involved. Out of the two-dimensional space of quasi-degenerate and weakly coupled *eg* and *ge* states, one can construct a state that maximally interacts with the *ac* and *tt* states, and a complementary orthogonal state that has negligible interactions with the two diabats. The S_3^d adiabat is more than 93% described by this complementary state at each R_{C-C}, giving it nearly pure local-exciton character.

The S_1^d, S_2^d, and S_4^d states deviate from the diabatic states that contribute to them at short R_{C-C} distances, demonstrating the importance of couplings between diabats in this region. The energy curve of the ground state S_0^d, which is not shown here (see Figure S.6), has a minimum at R_{C-C} = 5.5 Å, much like the excited states. This distance is shorter than the separation of 5.9 Å in the film structure, because our dimer model lacks the attraction between the surrounding pentacenes and the dimer ones, which increases R_{C-C}.

The relatively large slopes of all excited state energies at large R_{C-C} (Figure 4a) suggest substantial electrostatic contributions to these energies. The two charge-transfer states should have more pronounced electrostatic interactions and we see this in their steeper slopes at large R_{C-C}, compared to the other diabatic states. At R_{C-C} = 5.6 Å, the *ac* diabat crosses the *eg* and *ge* ones and becomes degenerate with the *tt* state at $R_{C-C} \leq 5.3$ Å (see Figure 4a). The superexchange mechanism of indirect *tt-eg/ge* coupling proposed by Berkelbach et al.[41] assumes an energy ordering of $E(tt) < E(eg) < E(ac)$ as well as the degeneracies $E(eg) = E(ge)$ and $E(ac) = E(ca)$.[68] This general model will require modification to describe SF in pentacene, especially at short R_{C-C}, where the *ac* diabat lies between the *tt* and *eg/ge* states and can mediate the mixing between them more effectively.

The couplings between the *ac* state and the other diabatic states vary substantially in magnitude, falling off with distance at large R_{C-C}. The *ca*-related couplings are of a similar magnitude (not shown in Figure 4b, but provided in Figure S.6), however, due to the large energy separation between *ca* and the other diabats these couplings can be ignored. The negligible Hamiltonian couplings in eq 4 continue to be small for all geometries and are not shown.

The magnitude ordering of the Hamiltonian couplings *eg-ac* > *tt-ac* > *ge-ac* is preserved for the entire range of R_{C-C}, as shown in Figure 4b. This can be explained by the orbital alignments in Figure 5, following the one-electron picture

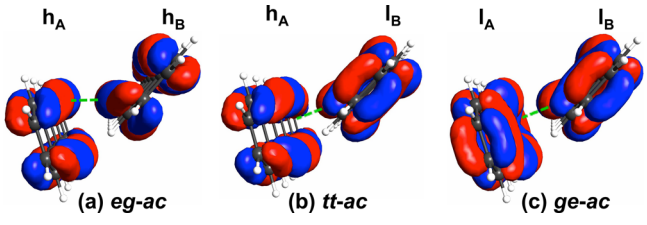

Figure 5. DMOs related to the Hamiltonian couplings of (a) *eg-ac*; (b) *tt-ac*; (c) *ge-ac*. The dimer takes the reference geometry. The green dashed lines highlight the directions of orbital interactions.

suggested by Smith and Michl.[2] In this picture, the three couplings are approximated by the integrals of $\langle h_A|\hat{F}|h_B\rangle$, $(3/2)^{1/2}\langle h_A|\hat{F}|l_B\rangle$, and $\langle l_A|\hat{F}|l_B\rangle$, where $\hat{F}$ is the Fock operator of the *gg* diabat. The orbital labels use *h* and *l* to represent the HOMO and LUMO, respectively, and the subscript indicates the monomer associated with the orbital. The orbital alignments in Figure 5 demonstrate that both h_B and l_B present a "σ-face" (single phase in the region of interaction) to interact with h_A and l_A. In Figure 5(a), h_B is "pointing" toward the upper edge of monomer A, where h_A has a large amplitude. Constructive interaction between h_A and h_B is responsible for the large magnitude of $\langle h_A|\hat{F}|h_B\rangle$. On the

dx.doi.org/10.1021/ja500887a | *J. Am. Chem. Soc.* 2014, 136, 5755−5764

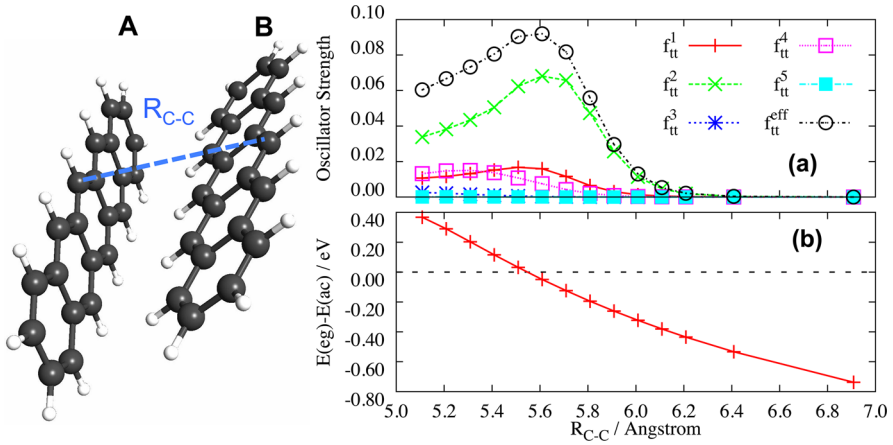

Figure 6. (a) Effective oscillator strength from the S_0^d state to the *tt* diabat (black circle) and contributions to it from the five adiabatic states (red plus, S_1^d; green cross, S_2^d; blue star, S_3^d; pink open square, S_4^d; cyan filled square, S_5^d); (b) The distance in energy between the *eg* and *ac* diabats as functions of R_{C-C}.

other hand, the protruding lobe of l_B toward monomer A points lower, more toward the nodal surface of h_A (Figure 5(b)) and where l_A has small amplitude (Figure 5(c)). This leads to a small magnitude of $\langle l_A|\hat{F}|l_B\rangle$ and an even smaller magnitude of $\langle h_A|\hat{F}|l_B\rangle$. We confirm this qualitative picture by calculating the three matrix elements, $\langle h_A|\hat{F}|h_B\rangle$ = 112 meV, $\langle h_A|\hat{F}|l_B\rangle$ = 80 meV, and $\langle h_A|\hat{F}|l_B\rangle$ = 91 meV at the reference geometry. Including the $(3/2)^{1/2}$ factor of the *tt-ac* coupling we obtain values of 112, 98, and 91 meV for the magnitudes of the one-electron approximate *eg-*, *tt-*, and *ge-ac* couplings. Translating monomer B along the $\mathbf{R}_{C-C}$ vector does not change the topology of orbital interactions in Figure 5, allowing the order in magnitude of these couplings to be maintained along the entire range of R_{C-C}.

In contrast to the pair of charge-transfer diabats, the pair of local-exciton states *eg* and *ge* stay close to each other, with their difference in energy <0.06 eV along the whole R_{C-C} range. The extent of their coupling with the *ac* state is therefore the only factor in determining which of them is more involved in the pentacene SF. Based on the analysis in the previous paragraph, one can see that the *eg* state is more strongly coupled to the *ac* state. The adiabatic S_1^d, S_2^d, and S_4^d states in eq 5 and Table 2, which contain considerable *tt* contributions, consistently have more contributions from the *eg* state than from the *ge* state.

The rapidly decreasing *ac* diabat and the increase in its coupling with the *tt*, *eg*, and *ge* states result in the adiabatic energies splitting apart as R_{C-C} decreases (Figure 4a). The crossing (or avoided crossing) of the adiabatic energy curves described in a previous work[47] is not observed in our calculations. Rather, we find that the effective mixing of the *tt*, *eg*, and *ge*, as shown by the $S_{1,2,4}^d$ states in eq 5, supports the coherent mechanism for SF proposed by Chan et al.[35,36]

Effective Oscillator Strengths for Transitions from the Ground State to the Multiexciton State. Although the *tt* diabatic state cannot be directly occupied through photoexcitation due to its zero transition dipole moment with the *gg* (S_0^d) state, in a coherent mechanism, the "dark" *tt* state is occupied through a coherent superposition with the "bright" *eg* or *ge* states. Beljonne et al. pointed out that this is equivalent to an intensity borrowing by the *tt* diabat from the *eg* or *ge*.[42] To quantify the coherent occupation of *tt* upon absorption of a photon, we define an "effective oscillator strength" from the ground state to the *tt* state as the sum over this diabat's share of the oscillator strengths, the sum extending and partitioned over the five low-lying S^d states,

$$f_{tt}^{\text{eff}} = \sum_{i=1}^{5} f_{tt}^{i} = \sum_{i=1}^{5} C_{i,tt}^2 f_i \tag{6}$$

Here $C_{i,tt}^2$ is the contribution of the *tt* diabat in the S_i^d adiabatic state, f_i the oscillator strength from the ground to the S_i^d state, and f_{tt}^i the component of adiabatic oscillator strength between S_0^d and S_i^d associated with the *tt* state. The oscillator strengths f_i are obtained by replacing the XMCQDPT treatment by the formally equivalent general multiconfigurational quasidegenerate perturbation theory (GMC-QDPT) for ease of implementation. We note that these two MRMP schemes exhibit similar accuracy, as verified by the <0.01 eV difference in excitation energies obtained from the two methods.

The f_{tt}^{eff} and its component f_{tt}^i's are plotted in Figure 6a as a function of R_{C-C}. A large value of f_{tt}^i requires both large values of $C_{i,tt}^2$ and significant magnitude for f_i. As described previously, f_i is substantial when the extent of *eg*/*ge* admixture is large in S_i^d. A delicate balance between the contributions of the *eg*, *ge*, and *tt* states to a given S_i^d state is thus essential to obtain large f_{tt}^i and f_{tt}^{eff} values. As R_{C-C} decreases, the magnitudes of f_{tt}^1, f_{tt}^2, and f_{tt}^{eff} start increasing at the reference geometry, R_{C-C} = 5.9 Å (the actual geometry in the film), and reach a maximum at about R_{C-C} = 5.6 Å. Figure 6a clearly shows that the major contribution to SF occurs by excitation to S_2^d, a state in which the *eg* and *ge* diabats dominate (more than 80%) at the reference structure. This state acquires more of the *tt* component as R_{C-C} shortens (a detailed comparison of the decompositions at R_{C-C} = 5.9, 5.6, and 5.1 Å is provided in Table S.3).

f_{tt}^{eff} maximizes at R_{C-C} = 5.6 Å, where there is the maximum mixing between the multi- (44.9%) and single-exciton (47.3%) diabats in S_2^d. As mentioned above, the *ac* and *eg*/*ge* diabatic energy curves cross in this region (Figure 4(a)), yielding the strongest *ac*-mediated *tt* and *eg*/*ge* mixing. As R_{C-C} further shortens, the *ac* diabat is separated in energy from *eg*/*ge* (Figure 6(b)). Consequently, the mediated mixing and f_{tt}^{eff} decrease. Evidently, a shorter intermolecular distance does not guarantee a more effective *tt* occupation.

With the lattice parameters of the pentacene crystal structure in use,[52] where R_{C-C} = 5.9 Å, we calculate the projections of the

dx.doi.org/10.1021/ja500887a | J. Am. Chem. Soc. 2014, 136, 5755−5764

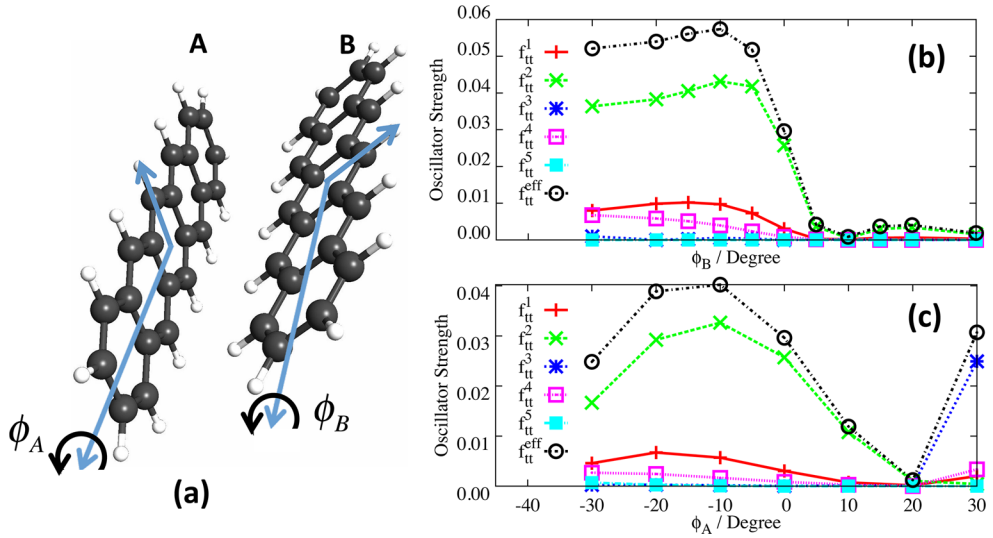

Figure 7. (a) Definition of the rotational angles ϕ_A and ϕ_B. (b) Effective oscillator strength from the S_0^d state to the *tt* diabat (black circle) and contributions to it from the five adiabatic states, as functions of the rotation of monomer B around its long axis (red plus, S_1^d; green cross, S_2^d; blue star, S_3^d; pink open square, S_4^d; cyan filled square, S_5^d). (c) Similar to (b), but for the rotation of monomer A.

$\mathbf{R}_{C-C}$ unit vector to be 0.5, 0.87 ($\sim\sqrt{3}/2$), and 0.15 on the *a*-, *b*-, and *c*-axes. We therefore predict that slightly compressing the pentacene crystal along the $\hat{a} + \sqrt{3}\hat{b}$ direction, to an $R_{C-C} \approx 5.6$ Å, is likely to enhance the *tt* occupation after photon absorption and consequently, the efficiency of the pentacene SF.

Structural Effects on the Pentacene Singlet Fission: Intermolecular Orientation. The highly anisotropic π-type frontier orbitals shown in Figure 5 suggest that intermolecular orientation is likely to significantly affect SF in pentacene. The orientational degree of freedom most likely to play a role is the rotation of the two monomers around their respective long-axes, shown in Figure 7a, since such rotation substantially changes the $\pi-\pi$ overlap.[11,69] To investigate this effect, we first rotate monomer B around its long axis and calculate the adiabatic and diabatic energies, diabatic couplings, and effective oscillator strength from the ground state to the *tt* state, as functions of the rotational angle. We define the rotational angle, ϕ_B, such that positive values indicate a counter-clockwise rotation. The rotational angle is constrained to vary from $-30°$ to $30°$, limiting our study to dimer configurations proximal to the reference geometry.

Figure 7b shows a dramatic dependence of f_{tt}^{eff} on ϕ_B. The *tt* effective oscillator strength vanishes for $\phi_B > 5°$ and maximizes for $\phi_B \approx -10°$. The maximum value of 0.06 is smaller than the maximum (0.09) in the R_{C-C} scanning. The detailed behavior of f_{tt}^{eff} can be understood on the basis of the orbital alignments of Figure 5, and the way the ensuing Hamiltonian couplings between the diabats evolve as a function of ϕ_B. This is detailed in Section S.4 in the SI; importantly, the *tt-ac* and *eg-ac* couplings increase as ϕ_B decreases from 0° and maximize at $\phi_B \sim 20°$.

A similar investigation probes the effect of rotating monomer A along its long axis by ϕ_A (defined in Figure 7a. Here a steric constraint enters; counter-clockwise rotation of monomer A "bumps" its lower edge into monomer B. Similarly to the case of ϕ_B, there is a rise of the *tt* effective oscillator strength as ϕ_A decreases and it maximizes at $\phi_A \approx -10°$, as shown in Figure 7c. The maximum f_{tt}^{eff} (0.04) is less than that of the ϕ_B rotation. The detailed analysis is again given in Section S.5 in the SI. An interesting feature is that f_{tt}^{eff} drops down to close to 0 as ϕ_A increases to about 20°, as the two monomers become perpendicular to each other, and rises up again as ϕ_A increases further.

Small clockwise rotations of monomer A or B around their long axes are, thus, shown to improve the efficiency of SF in pentacene. In practice, the orientation might be modified by introducing some bulky substituent along the long edge of pentacene molecule, however, this may at the same time enlarge the intermolecular distance (i.e., R_{C-C}) and conversely reduce the *tt* occupation. It would appear that adjusting the intermolecular distance may provide a better way to tune SF efficiency.

CONCLUSIONS

We have presented a thorough quantum chemistry study of the pentacene monomer and dimer. Our calculations are based on the well-developed MRMP scheme, which can treat both nondynamical and dynamical electron correlations accurately and cost-effectively. For the monomer, we put our effort into obtaining theoretically the correct energy order of pentacene's excited states. It is likely that the previously reported[25] (and subsequently disputed)[1,2] energy ordering of the lowest two singlet excited states is a result of an intruder state problem; with a proper active space, an order of $E(S_1) < E(D)$ is obtained that is consistent with experimental observations. We also show that a minimum active space, containing only the HOMO and LUMO of the molecule, yields satisfactory MRMP excitation energies. The success of this monomer active space encourages us to use the minimum 4o4e space in the subsequent dimer calculations.

We construct a dimer model that mimics the unit cell structure of the pentacene crystal. We then employ the well-developed four-fold diabatization scheme to analyze the excited states of the dimer and investigate the roles of the low-lying diabats in the process of SF. The Hamiltonian matrix in the basis of the diabatic states indicates that there is little direct interaction between the multi- and single-exciton states and that they are indirectly coupled through a charge-transfer state. This provides further confirmation of the indirect SF

dx.doi.org/10.1021/ja500887a | J. Am. Chem. Soc. 2014, 136, 5755−5764

mechanism proposed by Smith and Michl[1,2] in pentacene. The involvement of the charge-transfer state induces effective mixing between the multi- and single-exciton diabats in the low-lying adiabatic states, supporting the coherent mechanism for rapid pentacene SF proposed by Chan et al.[35] We find that only one of the two charge-transfer states, *ac*, is engaged in the SF in pentacene; it is the low-lying charge-transfer state that gets closer to the multi- and single-exciton states. Moreover, the *ac* diabat can move into degeneracy with the single-exciton states, more effectively mediating the mixing of the bright single- to and dark multiexciton diabats. This finding is different from the basic assumption of high-lying charge-transfer states in the superexchange model, emphasizing the need to adapt the general SF model to specific cases.

We quantify the population of the singlet coupled multiexciton state after absorbing a photon by defining an effective oscillator strength for this state and computing it as a function of dimer structure. Dimer structures with exceptionally high values of the effective oscillator strength are identified. Among these, a structure with a reduced intermolecular distance is especially appealing for improving SF efficiency, since it can be realized by compressing the pentacene crystal along a certain direction.

COMPUTATIONAL METHODS

The necessity of treating both the multireference nature of their wave functions and dynamical correlation for acene molecules has been established by Hirao et al.[23,24] Following their calculations for the shorter acenes and Zimmerman et al.'s work on pentacene,[25] we apply MRMP-based methods to calculate the wave functions and energies of the low-lying electronic states of the pentacene molecule. We employ the cc-pVTZ basis set[70] in our monomer calculations; the basis set is trimmed to reduce computational cost, i.e., the *f* basis functions of carbon and *d* functions of hydrogen are removed.[25] The MRMP calculations for pentacene monomer are carried out using the GMC-QDPT developed by Nakano et al.[54,71,72] For the MRMP/2o2e calculation of vertical excitation energies of pentacene molecule, the CASSCF/12π12e optimized ground state structure is used. Intruder state avoidance (see text) is employed with the conventional shifting parameter of 0.02 E_H^2.[56] The same parameter is used in all ISA treatments in this work. The zeroth-order states are prepared in a state-averaged CASSCF manner.

The larger size and lower symmetry (C_1) of the dimer require us to use a smaller basis set. We employ the SBKJC[73,74] pseudopotential and its associated double-ζ basis set for the dimer calculations. The *d* function from the 6-31G(d) basis set of carbon is added to account for polarization. This combined basis set is of similar quality to the 6-31G(d) basis which was used in a previous dimer study,[47] for the valence electrons. The carbon core 1s electrons are replaced by a pseudopotential. The same basis set and pseudopotential are used in the MRMP/2o2e calculation for the vertical excitation energies of pentacene monomer.

The XMCQDPT method of Granovsky[75] is used to handle both the nondynamical and dynamical correlation for the dimer. Since dynamical electron correlation is explicitly included, we do not adjust the state energies as is done in refs 45 and 47. All GMC-QDPT calculations in this work also use Granovsky's XMCQDPT zeroth-order Hamiltonian to have reasonable interactions between the zeroth-order states.

All calculations are carried out using the quantum chemistry program package GAMESS-US.[76,77] Its associated graphical software MacMolPlt[78] is used to prepare all the molecular geometry and orbital images in this paper.

ASSOCIATED CONTENT

Supporting Information

Figures S.1−S.10; Tables S.1−S.3; all calculation results of pentacene monomer with detailed discussion; discussion on the energy difference between the *ac* and *ca* diabats and on the *ca* diabat along R_{C-C}; analysis of the *tt* effective oscillator strength as functions of ϕ_B and ϕ_A; coordinates and absolute energies for the petacene monomer S_0 state, the pentacene monomer T_1 state, and the pentacene dimer reference structure.

This material is available free of charge via the Internet at http://pubs.acs.org.

AUTHOR INFORMATION

Corresponding Author

ananth@cornell.edu

Notes

The authors declare no competing financial interest.

ACKNOWLEDGMENTS

We are grateful to Professor Paul Zimmerman for sharing with us his GAMESS-US inputs and pentacene monomer coordinates. We need to thank Professor Neil Ashcroft for enlightening discussions. We also thank Professor Mark Gordon and Dr. Michael Schmidt for their continuing development of the GAMESS-US program suite. T.Z. is especially thankful to Dr. Schmidt for his implementation of the fourfold diabatization scheme into GAMESS-US. T.Z. expresses his gratitude to the Natural Sciences and Engineering Research Council of Canada for the Banting postdoctoral fellowship (201211BAF-303459-236530). R.H. is grateful to the National Science Foundation for its financial support (CHE-1305872). N.A. is grateful for the support of a start-up grant from Cornell University.

REFERENCES

(1) Smith, M. B.; Michl, J. *Chem. Rev.* **2010**, *110*, 6891−6936.
(2) Smith, M. B.; Michl, J. *Annu. Rev. Phys. Chem.* **2013**, *64*, 361−386.
(3) Shockley, W.; Queisser, H. J. *J. Appl. Phys.* **1961**, *32*, 510−519.
(4) Hanna, M. C.; Nozik, A. J. *J. Appl. Phys.* **2006**, *100*, 074510.
(5) Paci, I.; Johnson, J. C.; Chen, X. D.; Rana, G.; Popović, D.; David, D. E.; Nozik, A. J.; Ratner, M. A.; Michl, J. *J. Am. Chem. Soc.* **2006**, *128*, 16546−16553.
(6) Congreve, D. N.; Lee, J.; Thompson, N. J.; Hontz, E.; Yost, S. R.; Reusswig, P. D.; Bahlke, M. E.; Reineke, S.; Van Voorhis, T.; Baldo, M. A. *Science* **2013**, *340*, 334−337.
(7) Singh, S.; Jones, W. J.; Siebrand, W.; Stoicheff, B. P.; Schneider, W. G. *J. Chem. Phys.* **1965**, *42*, 330−342.
(8) Swenberg, C. E.; Stacy, W. T. *Chem. Phys. Lett.* **1968**, *2*, 327−328.
(9) Groff, R. P.; Avakian, P.; Merrifield, R. E. *Phys. Rev. B* **1970**, *1*, 815−817.
(10) Greyson, E. C.; Stepp, B. R.; Chen, X.; Schwerin, A. F.; Paci, I.; Smith, M. B.; Akdag, A.; Johnson, J. C.; Nozik, A. J.; Michl, J.; Ratner, M. A. *J. Phys. Chem. B* **2010**, *114*, 14223−14232.
(11) Kuhlman, T. S.; Kongsted, J.; Mikkelsen, K. V.; Møller, K. B.; Sølling, T. I. *J. Am. Chem. Soc.* **2010**, *132*, 3431−3439.
(12) Wolf, H. C. *Solid State Phys.* **1959**, *9*, 1−81.
(13) Avakian, P.; Abramson, E.; Kepler, R. G.; Caris, J. C. *J. Chem. Phys.* **1963**, *39*, 1127−1128.
(14) Tomkiewicz, Y.; Groff, R. P.; Avakian, P. *J. Chem. Phys.* **1971**, *54*, 4504−4507.
(15) Sebastian, L.; Weiser, G.; Bässler, H. *Chem. Phys.* **1981**, *61*, 125−135.
(16) Lee, K. O.; Gan, T. T. *Chem. Phys. Lett.* **1977**, *51*, 120−124.
(17) Burgos, J.; Pope, M.; Swenberg, C. E.; Alfano, R. R. *Phys. Status Solidi. B* **1977**, *83*, 249−256.

(18) Rao, A.; Wilson, M. W. B.; Hodgkiss, J. M.; Albert-Seifried, S.; Bässler, H.; Friend, R. H. *J. Am. Chem. Soc.* **2010**, *132*, 12698−12703.
(19) Rao, A.; Wilson, M. W. B.; Albert-Seifried, S.; Di Pietro, R.; Friend, R. H. *Phys. Rev. B* **2011**, *84*, 195411.
(20) Wilson, M. W. B.; Rao, A.; Clark, J.; Kumar, R. S. S.; Brida, D.; Cerullo, G.; Friend, R. H. *J. Am. Chem. Soc.* **2011**, *133*, 11830−11833.
(21) Wilson, M. W. B.; Rao, A.; Ehrler, B.; Friend, R. H. *Acc. Chem. Res.* **2013**, *46*, 1330−1338.
(22) Pabst, M.; Köhn, A. *J. Chem. Phys.* **2008**, *129*, 214101.
(23) Hashimoto, T.; Nakano, H.; Hirao, K. *J. Chem. Phys.* **1996**, *104*, 6244−6257.
(24) Kawashima, Y.; Hashimoto, T.; Nakano, H.; Hirao, K. *Theor. Chem. Acc.* **1999**, *102*, 49−64.
(25) Zimmerman, P. M.; Zhang, Z.; Musgrave, C. B. *Nat. Chem.* **2010**, *2*, 648−652.
(26) Hirao, K. *Chem. Phys. Lett.* **1990**, *190*, 374−380.
(27) Hirao, K. *Chem. Phys. Lett.* **1992**, *196*, 397−528.
(28) Hirao, K. *Chem. Phys. Lett.* **1993**, *201*, 59−66.
(29) Amirav, A.; Even, U.; Jortner, J. *Chem. Phys. Lett.* **1980**, *72*, 21−24.
(30) Griffiths, A. M.; Friedman, P. A. *J. Chem. Soc., Fraday Trans. 2* **1982**, *78*, 391−398.
(31) Merrifield, R. E. *J. Chem. Phys.* **1968**, *48*, 4318.
(32) Johnson, R.; Merrifield, R. *Phys. Rev. B* **1970**, *1*, 896−902.
(33) Suna, A. *Phys. Rev. B* **1970**, *1*, 1716−1739.
(34) Chan, W.-L.; Ligges, M.; Zhu, X.-Y. *Nat. Chem.* **2012**, *4*, 840−845.
(35) Chan, W.-L.; Ligges, M.; Jailaubekov, A.; Kaake, L.; Miaja-Avila, L.; Zhu, X.-Y. *Science* **2011**, *334*, 1541−1545.
(36) Chan, W.-L.; Berkelbach, T. C.; Provorse, M. R.; Monahan, N. R.; Tritsch, J.; Hybertsen, M. S.; Reichman, D. R.; Gao, J.; Zhu, X.-Y. *Acc. Chem. Res.* **2013**, *46*, 1321−1329.
(37) Greyson, E. C.; Vura-Weis, J.; Michl, J.; Ratner, M. A. *J. Phys. Chem. B* **2010**, *114*, 14168−14177.
(38) Yamagata, H.; Norton, J.; Hontz, E.; Olivier, Y.; Beljonne, D.; Brédas, J. L.; Silbey, R. J.; Spano, F. C. *J. Chem. Phys.* **2011**, *134*, 204703.
(39) Teichen, P. E.; Eaves, J. D. *J. Phys. Chem. B* **2012**, *116*, 11473−11481.
(40) Berkelbach, T. C.; Hybertsen, M. S.; Reichman, D. R. *J. Chem. Phys.* **2013**, *138*, 114102.
(41) Berkelbach, T. C.; Hybertsen, M. S.; Reichman, D. R. *J. Chem. Phys.* **2013**, *138*, 114103.
(42) Beljonne, D.; Yamagata, H.; Brédas, J. L.; Spano, F. C.; Olivier, Y. *Phys. Rev. Lett.* **2013**, *110*, 226402.
(43) Difley, S.; Van Voorhis, T. *J. Chem. Theory Comput.* **2011**, *7*, 594−601.
(44) Havenith, R. W. A.; de Gier, H. D.; Broer, R. *Mol. Phys.* **2012**, *110*, 2445−2454.
(45) Feng, X.; Luzanov, A. V.; Krylov, A. I. *J. Phys. Chem. Lett.* **2013**, *4*, 3845−3852.
(46) Kolomeisky, A. B.; Feng, X.; Krylov, A. I. *J. Phys. Chem. C* **2014**, *118*, 5188−5195.
(47) Zimmerman, P. M.; Bell, F.; Casanova, D.; Head-Gordon, M. *J. Am. Chem. Soc.* **2011**, *133*, 19944−19952.
(48) Zimmerman, P. M.; Musgrave, C. B.; Head-Gordon, M. *Acc. Chem. Res.* **2013**, *46*, 1339−1347.
(49) Heinecke, E.; Hartmann, D.; Muller, R.; Hese, A. *J. Chem. Phys.* **1998**, *109*, 906−911.
(50) Thorsmølle, V. K.; Averitt, R. D.; Demsar, J.; Smith, D. L.; Tretiak, S.; Martin, R. L.; Chi, X.; Crone, B. K.; Ramirez, A. P.; Taylor, A. J. *Phys. Rev. Lett.* **2009**, *102*, 017401.
(51) Thorsmølle, V. K.; Averitt, R. D.; Demsar, J.; Smith, D. L.; Tretiak, S.; Martin, R. L.; Chi, X.; Crone, B. K.; Ramirez, A. P.; Taylor, A. J. *Physica B* **2009**, *404*, 3127−3130.
(52) Schiefer, S.; Huth, M.; Dobrinevski, A.; Nickel, B. *J. Am. Chem. Soc.* **2007**, *129*, 10316−10317.
(53) Nakano, H.; Nakayama, K.; Hirao, K. *J. Chem. Phys.* **1996**, *106*, 4912−4917.
(54) Ebisuzaki, R.; Watanabe, Y.; Nakano, H. *Chem. Phys. Lett.* **2007**, *442*, 164−169.
(55) Choe, Y.-K.; Witek, H. A.; Finley, J. P.; Hirao, K. *J. Chem. Phys.* **2001**, *114*, 3913−3918.
(56) Witek, H. A.; Choe, Y.-K.; Finley, J. P.; Hirao, K. *J. Comput. Chem.* **2002**, *23*, 957−965.
(57) Schulten, K.; Karplus, M. *Chem. Phys. Lett.* **1972**, *14*, 305−309.
(58) Hosteny, R. P.; Dunning, T. H.; Gilman, R. R.; Pipano, A.; Shavitt, I. *J. Chem. Phys.* **1975**, *62*, 4764−4779.
(59) Akimov, A. V.; Prezhdo, O. V. *J. Am. Chem. Soc.* **2014**, *136*, 1599−1608.
(60) Ruedenberg, K.; Atchity, G. J. *J. Chem. Phys.* **1993**, *99*, 3799−3803.
(61) Nakamura, H.; Truhlar, D. G. *J. Chem. Phys.* **2011**, *115*, 10353−10372.
(62) Nakahara, H.; Truhlar, D. G. *J. Chem. Phys.* **2002**, *117*, 5576−5593.
(63) Ichino, T.; Gauss, J.; Stanton, J. F. *J. Chem. Phys.* **2009**, *130*, 174105.
(64) Köppel, H.; Domcke, W.; Cederbaum, L. S. *Adv. Chem. Phys.* **1984**, *59*, 57−246.
(65) Prikhotko, A. F.; Tsikora, L. I. *Opt. Spectrosc.* **1968**, *25*, 242.
(66) Zanker, V.; Preuss, J. *Z. Angew. Phys.* **1969**, *27*, 363.
(67) Yamagata, H.; Norton, J.; Hontz, E.; Olivier, Y.; Beljonne, D.; Brédas, J. L.; Silbey, R. J.; Spano, F. C. *J. Chem. Phys.* **2011**, *134*, 204703.
(68) This assumption is only valid if the two monomers are symmetrically positioned.
(69) Marciniak, H.; Fiebig, M.; Huth, M.; Schiefer, S.; Nickel, B.; Selmaier, F.; Lochbrunner, S. *Phys. Rev. Lett.* **2007**, *99*, 176402.
(70) Dunning, T. H. *J. Chem. Phys.* **1989**, *90*, 1007−1023.
(71) Nakano, H.; Uchiyama, R.; Hirao, K. *J. Comput. Chem.* **2002**, *23*, 1166−1175.
(72) Miyajima, M.; Watanabe, Y.; Nakano, H. *J. Chem. Phys.* **2006**, *124*, 044101.
(73) Binkley, J. S.; Pople, J. A.; Hehre, W. J. *J. Am. Chem. Soc.* **1980**, *102*, 939−947.
(74) Stevens, W. J.; Basch, H.; Krauss, M. *J. Chem. Phys.* **1984**, *81*, 6026−6033.
(75) Granovsky, A. A. *J. Chem. Phys.* **2011**, *134*, 214113.
(76) Schmidt, M. W.; Baldridge, K. K.; Boatz, J. A.; Elbert, S. T.; Gordon, M. S.; Jensen, J. H.; Koseki, S.; Matsunaga, N.; Nguyen, K. A.; Su, S.; Windus, T. L.; Dupuis, M.; Montgomery, J. A., Jr. *J. Comput. Chem.* **1993**, *14*, 1347−1363.
(77) Gordon, M. S.; Schmidt, M. W. In *Advances in electronic structure theory: GAMESS a decade later*; Dykstra, C. E., Frenking, G., Kim, K. S., Scuseria, G. E., Eds.; Elsevier: Amsterdam, 2005.
(78) Bode, B. M.; Gordon, M. S. *J. Mol. Graphics Modell.* **1998**, *16*, 133−138.

JACS
JOURNAL OF THE AMERICAN CHEMICAL SOCIETY
Spotlights
pubs.acs.org/JACS

Spotlights on Recent *JACS* Publications

SYNTHETIC PEPTIDE SCORES MORE PORES FOR DRUG DELIVERY

William Wimley and colleagues report a synthetic peptide that creates long-lived macromolecule-sized pores in a lipid bilayer membrane (DOI: 10.1021/ja500462s). The work could support a host of biotechnology applications, including drug delivery.

To deliver a large or polar drug into a cell, researchers need a way to breach the cell membrane. One promising approach is to introduce peptides that self-assemble into pores in the lipid bilayer membrane. But scientists have struggled to find or design peptides that potently form and maintain these pores for an extended period of time. Now Wimley and co-workers have synthetically evolved a peptide that fits the bill. They take a bee venom peptide that forms transient membrane pores and make modifications to several of its residues. Then they screen the ensuing variants for their pore-forming ability.

The team identifies a peptide that introduces multiple, long-lasting pores with very low concentrations of peptide. The pores are large enough for a macromolecule to pass through. The advance could be used as a platform for many applications in biotechnology, including drug delivery, targeted cancer and HIV therapies, and biosensor development.

Deirdre Lockwood, Ph.D.

PROTECTIVE ELECTROCHEMICAL N-FUNCTIONALIZATION OF IMIDAZOLES

When Michael Faraday established the foundation of electrochemistry nearly two centuries ago, he would probably have never imagined how widely used it would become. As an elegant example of electrochemical organic synthesis, Jun-ichi Yoshida and co-workers have recently developed a convenient approach to N-functionalized imidazoles by electrooxidative activation of aryl and benzylic compounds (DOI: 10.1021/ja501093m).

Activating unreactive C−H bonds is a highly sought-after target within the community of synthetic methodology, which electrochemical methods can rarely be harnessed to achieve. For instance, overoxidation presents an obstacle in the case of direct C−N coupling between imidazoles and aryl or benzylic compounds via anodic oxidation. However, the authors provide an ingenious solution to this problem by introducing a protecting group to imidazoles, which renders the products nonsusceptible to side reactions.

The versatile utility of this strategy is demonstrated by the easy syntheses of two bioactive N-substituted imidazole derivatives. Being chemoselective and metal-free, it dramatically simplifies the transformation that would otherwise require prefunctionalization and metal catalysts.

Xin Su, Ph.D.

ENHANCING SOLAR CELL EFFICIENCY WITH SINGLET FISSION IN PENTACENE

The maximum efficiency of single-junction solar cells is 33.7%, the so-called Shockley−Queisser limit. Singlet fission, a process that generates two excitons from one excited singlet state after absorbing one photon, could be the key to push the efficiency beyond this limit. Tao Zeng, Roald Hoffmann, and Nandini Ananth present a detailed quantum chemistry study of pentacene monomer and dimer that serves to reconcile existing views of the singlet fission process and gives a clearer picture of the mechanism (DOI: 10.1021/ja500887a).

Using a computational method that can accurately handle both nondynamical and dynamical electron correlations, the team calculates the electronic states of pentacene monomer and dimer. The authors characterize the six low-lying singlet states of a pentacene dimer at geometries that approximate the unit cell structure of crystalline pentacene and elucidate the roles of these six states in singlet fission. Study of structural effects on singlet fission in the pentacene dimer suggests a significant dependence of the efficiency of singlet fission on intermonomer distance and orientation.

Hui Jin, Ph.D.

COLOR CODERS GET A BOOST

Biological researchers rely heavily on molecular tagging to determine where cells and molecules go and how they interact. Luminescent dots work well for tagging, but sometimes researchers need more options. So-called biological barcodes add a layer of complexity, incorporating multiple colors and patterns into a light-emitting tag. A biological barcode needs to be bright, distinct, abundant, versatile, and low-cost. Unfortunately, current choices rarely meet all these needs.

Xiaogang Liu and colleagues contribute a valuable addition to the toolbox with multicolor barcodes based on lanthanide crystal rods (DOI: 10.1021/ja5013646). Through a process called upconversion, lanthanide crystals can convert longer wavelength, lower energy light into higher energy, visible wavelengths. This property is ideal for observing delicate cells and tissues without causing damage.

The researchers vary the rods' composition from the center to the ends so that the rods emit different patterns of red, green, and blue light. The crystals are low-cost, bright, long-lasting, and size-flexible and can be created in large batches. In experiments the glowing rods were easily readable with a conventional optical microscope. In addition to cell tracking, these materials would make excellent optical barcodes for anticounterfeiting and security applications.

Jenny Morber, Ph.D.

ISOBUTANOL: A FURTHER STEP TOWARD MODELING ITS COMBUSTION

Donald Truhlar and co-workers have described, using several new developments in computational chemistry, essential parameters related to the combustion of isobutanol (DOI: 10.1021/ja5011288). Isobutanol, $(CH_3)_2CHCH_2OH$, which can be obtained by the fermentation of carbohydrates, is of interest as a biofuel because it has combustion properties close

Published: April 1, 2014

dx.doi.org/10.1021/ja503143p | *J. Am. Chem. Soc.* 2014, 136, 5179−5180

to that of gasoline, and also because it can be blended with gasoline.

Modeling the combustion mechanism of isobutanol requires reliable values of the reaction rates for the abstraction reactions of a hydrogen atom from each of four distinguishable sites by hydroxyl radicals (OH). The four kinds of hydrogen atoms are attached to the carbon atom of one of the methyl groups, to the two remaining carbon atoms of the molecule, and to the oxygen atom of the hydroxyl group. However, experimental determinations of the reaction rates have remained inconclusive because of many secondary reactions as well as difficulties in detecting product radicals, while previous computations were affected by various kinds of errors.

Here, the researchers have determined the individual rate constants of each of the four abstraction reactions and the branching ratios by applying variational transition-state theory. Taking into account a large number of factors, including conformations of transition structures, barrier heights, tunnelling transmission coefficients, anharmonicity in zero-point energy, and in torsional vibrational modes, they obtain values for the four reaction rate constants as a function of temperature. The results agree with available experiments for the sum of the rate constants over wide ranges of temperature, but also supply the experimentally missing branching ratios.

Alexander Hellemans

dx.doi.org/10.1021/ja503143p | *J. Am. Chem. Soc.* 2014, 136, 5179−5180